ISSN 1392-1207. MECHANIKA. Vol. 32, No. 2, 2026: 92–99

Study on the Creep Deformation Characteristics of the Cylindrical Tubes under External Pressure

Ming ZHANG*,, Shiqi LI*,**, Zhongqiang FENG*,**, Mingjiang HAN***, Bei ZHANG*,****

**School of Automotive Engineering, Hubei University of Automotive Technology, Shiyan, Hubei, China, 442002, E-mails: m15822046551@163.com (Ming Zhang), li122625@petalmail.com (Shiqi Li), fzqrsyj@163.com (Zhongqiang Feng), zhangbei_2012@163.com (Bei Zhang), (Corresponding authors: Bei Zhang and Mingjiang Han)*

***Key Laboratory of Automotive Power Train and Electronics, Hubei University of Automotive Technology, Shiyan, Hubei, China, 442002*

****Army Engineering University of PLA, Shijiazhuang, Hebei, China, 050050, E-mail: mjhan@tju.edu.cn*

https://doi.org/10.5755/j02.mech.43236

1. Introduction

The nuclear fuel cladding will undergo continuous inward creep deformation after long-term service in extreme environments of high temperature, high pressure, and strong fast neutron irradiation. The axial height of the pellets becomes shorter because of the densification effect in the early stage of irradiation [1], and there may be an axial gap between the pellets and the cladding, resulting in unsupported segments in the cladding. The inward creep rate of the unsupported section of the cladding will further increase due to temperature and radiation effects, which may lead to creep collapse failure of the cladding [2]. The failure of the cladding structure will directly lead to the leakage of radioactive substances and cause changes in the coolant flow channel, which poses a risk of bending adjacent fuel rods and guide tubes, seriously affecting the safety of pressurized water reactor operation [3]. The design standards for pressurized water reactor fuel assemblies stipulate that the cladding should not experience creep collapse throughout the entire design life [4]. Therefore, predicting the creep deformation of the cladding tube is the key to evaluating whether the cladding tube collapses or suffers excessive creep deformation.

It is difficult to monitor the deformation behavior of the cladding directly under complex service conditions inside the reactor. In order to predict the creep behavior of cladding under various factors such as heat, force, and neutron irradiation, specialized software such as BUCKLE [5], COLAPX [6], COVE-1 [7], CEPAN [8], FROCO [9], etc. have been developed in the field of nuclear fuel rods. However, the software above is based on the assumption of two-dimensional plane strain, and its geometric model is an infinitely long tube (plane strain hypothesis), which differs from the actual deformation mode of a three-dimensional finite-length tube. Although COLAPX [6], COVE [7], CEPAN [8], and FROCO [9] try to adopt the correction coefficients to obtain three-dimensional creep deformation from the predicted results of the two-dimensional model to reduce the deviation between the calculated results and the actual deformation. However, the method of correcting the three-dimensional model deformation from the two-dimensional model results has natural shortcomings, especially when the tube length is short, it is difficult to capture the complex three-dimensional creep phenomenon of the cladding tube.

In the early stage, Hoff, Bargmann, and Nishiguchi [17-19] proposed analytical calculation methods for creep under external pressure on long tubes, but the applicability of analytical solutions for finite-length cladding tubes needs to be studied. With the continuous maturity and development of commercial 3D finite element analysis software, scholars have utilized the ABAQUS [21] and ANSYS [22] with its user subroutines, which can achieve more accurate simulation of the creep behavior of 3D fuel rod cladding. Zhang Xiaodi et al. [10] used the finite element software ABAQUS and its subroutines to study the deformation and stress distribution of the cladding under creep and irradiation, respectively, demonstrating the applicability of ABAQUS in fuel rod creep and irradiation growth conditions. Zhang Ming et al. [11] studied the three-dimensional creep collapse behavior of coated cladding tubes based on the solid element of commercial software ABAQUS and considered the influence of irradiation growth in nuclear reactors on the creep collapse of cladding tubes [12]. Tang Changbing et al. [13] introduced the thermal and irradiation effects of fuel rods into the calculation based on ABAQUS and simulated the radiation thermal mechanical coupling performance of fuel rods under steady-state and transient conditions. The above analysis method based on commercial finite element software has reliable calculation results and high calculation efficiency, but it has not analyzed the creep deformation characteristics of the cladding tube structure, nor has it summarized the deformation characteristics of the metal tube structure under external pressure creep. A detailed mechanical modeling focus on the creep deformation characteristics and its relative parametric study has not been seen in the literature till now. This study establishes a three-dimensional mechanical modeling of the cladding structure, analyzes the influence of different geometric parameters and boundary conditions on the creep deformation of the cladding tube under external pressure, and provides a reference for the prediction of creep deformation, which will be helpful to the behavior-prediction and geometry-design of the claddings.

The second section describes the modeling method of cladding tubes based on ABAQUS, the third section analyzes and discusses the calculation results, and the last section summarizes the creep deformation characteristics of the cladding tubes and states the limitations of the current study.

2. Methodology

The commercial finite element software ABAQUS [21] is utilized to establish a finite element model of the

cladding tube, and its subroutine CREEP is developed to simulate the steady-state creep effect.

2.1. Geometry and material model of the cladding

In the baseline model of this study, the geometric parameters of the cladding tube used are: 9.5 mm of the outer diameter, 0.57 mm of the thickness, and 20 mm of the axial length. Considering manufacturing defects or errors, it is assumed that the cross-section of the cladding tube is not circular, but an ellipse with a certain initial ovality OV0. Ovality is defined as the difference between the outer diameter of the major axis and the outer diameter of the minor axis of the elliptical cross-section, as shown in Fig. 1. The initial ovality OV0 = 0.064 mm will utilize the baseline model.

The material of the cladding tube is selected as zirconium alloy. For the convenience of analysis, the stress is not very high thus an isotropic linear elastic material is sufficient to represent its behavior for the creep deformation analysis. This paper does not focus on the influence of material parameters on the creep deformation of the cladding tube. Therefore, Young's modulus and Poisson's ratio are constants, where Young's modulus is taken as 79800 MPa and the Poisson's ratio is taken as 0.34. The yield strength of the zirconium alloy is taken as 500 MPa [11].

The total creep is the combination of thermal creep and irradiation creep. The creep constitutive laws in the rate form are

$$\dot{\varepsilon}_{total} = \dot{\varepsilon}_{th} + \dot{\varepsilon}_{irr}$$
$$\dot{\varepsilon}_{th} = A\frac{E}{T}\left(sinh\frac{a_i\sigma_{eff}}{E}\right)^n exp\left(-\frac{Q}{RT}\right). \quad (1)$$
$$\dot{\varepsilon}_{irr} = C_0\phi^{C_1}\sigma^{C_2} f(T)$$

Parameters of Eq. (1) are shown in Table 1.

The irradiation-induced axial growth must be considered in the long-term simulation, which is a function of the neutron flux with the following rate form

Table 1

Creep parameters of the zirconium alloy form [12, 16]

Parameter	Unit	Value
A	K·(MPa·h)$^{-1}$	1.08×10^9
E	MPa	$1.149\times10^5 - 59.9\times T$
	MPa^{-1}	$650\left[1-0.56\left(1-e^{-1.4\times10^{-27}\phi^{1.3}}\right)\right]$, ϕ is a fluence, n/cm^2
n	–	2.0
Q	kJ·mol^{-1}	201
R	kJ·(mol·K)$^{-1}$	0.008314
C_0	(n·m^{-2}·s^{-1})$^{-C_1}$ ·MPa$^{-C_2}$	4.0985×10^{-24}
C_1	–	0.85
C_2	–	1.0
$f(T)$	–	$T < 570$ K: 0.7283 $570 \le T \le 625$ K: $-7.0237+0.0136T$ $T > 625$ K: 1.4763

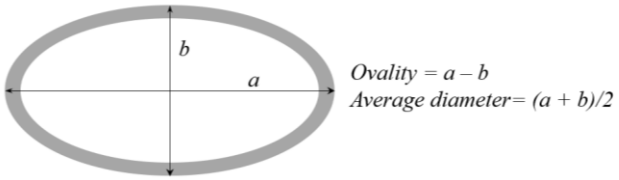

Fig. 1 Definition of the ovality and average diameter of the elliptical section

$$\dot{\varepsilon}_{grow} = 0.00075\cdot\phi\cdot10^{-21}. \quad (2)$$

2.2. Analysis model

For long-term cumulative creep problems, transient effects can be ignored, so the VISCO solver of ABAQUS is utilized to solve quasi-static creep problems. Before analysis, the model was ensured to meet the mesh-independent test by adjusting the mesh density. In the CREEP subroutine, the thermal creep model, irradiation creep model and irradiational growth model are integrated (Eqs. (1) and (2)).

2.3. Loadings and boundary conditions

The pressure of the pressurized water reactor is 15.5 MPa, and the inner pressure of pre-filled helium is between 2 and 3 MPa. Thus, the pressure difference is set to be 13 MPa and set constant during the life (Fission gas release is ignored for conservative purposes). The

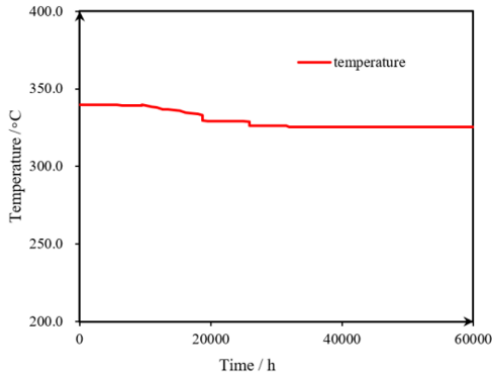

a

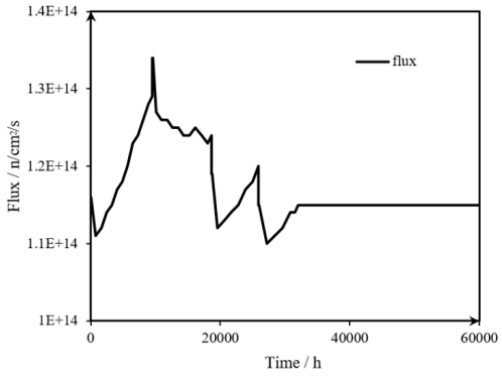

b

Fig. 2 Temperature history and flux history of the cladding tube: a – temperature history, b – flux history

displacement boundary conditions see Sec. 3.4 for detail. A typical temperature and flux history are shown in Fig. 2.

Considering that the cladding tube is restricted by the grid spring within the fuel assembly, and the unsupported section of the cladding tube is part of the entire cladding, attention should be paid to the selection of its end boundary conditions. In the baseline, a boundary condition with fixed displacement at both ends is adopted, and the effects of different boundary conditions will be compared later.

3. Results and Discussions

3.1. Baseline results

For the baseline model, it can be seen that as the service time increases, the creep deformation becomes larger. When $t = 60000$ h, the ovality reaches 0.76 mm as shown in Fig. 3. The displacements of the long and short axis endpoints A and B (U_A and U_B on Fig. 3 are u_A and v_B due to the strict definition of mechanics, and negative displacement indicates inward deformation) are both towards the interior of the pipeline, indicating that the cladding wall is compressed in the circumferential direction. The equivalent stress and displacement contours at this time are shown in Fig. 4, c), with a maximum stress of 112.7 MPa and a maximum displacement of 0.4 mm.

3.2. Effects of cladding tube length

Generally speaking, the axial length of the cladding tube will affect its deformation characteristics. This section conducts a sensitivity study on the length of the cladding tube.

The axial lengths of the cladding tube were set to 10 mm, 15 mm, 20 mm (baseline), 40 mm, 80 mm, 200 mm, and 400 mm, respectively. Fig. 4 shows the mises stress contour and displacement contour of the cladding tube. The comparison of their ovality-time curve is shown in Fig. 5, and the creep deformation of the major axis (point A in Fig. 2) and minor axis (point B in Fig. 2) are shown in Fig. 6.

From Fig. 5, it can be seen that as the axial length of the tube increases, the final ovality becomes larger. For tubes with axial length < 20 mm, the ovality-time curve shows a concave trend; When the axial length is greater than 40 mm, its ovality-time curve shows an upward convex trend and will collapse in a short period due to excessive deformation. When the length of the cladding tube is greater than 200 mm, increasing the axial length has no significant effect on the ovality-time curve (curves of the long 200 mm and 400 mm coincide). That is, from the perspective of creep deformation prediction, when the length diameter ratio is over 21 ($H/D = 200/9.5 = 21.05$), the tube can be seen as infinite-length tube and the plane strain hypothesis is reasonable and valid. For the tubes with sufficient long axial length (long ≥ 40 mm, length diameter ratio $H/D \geq 40/9.5 = 4.2$), the creep deformation shows similar characteristics, and the creep deformation can be corrected by the factor from the infinite long tube in the software CROV [15] and FROCO [9].

The displacement of points A (on the major axis) and B (on the minor axis) in the middle section of the cladding tube is shown in Fig. 6, a and b. It can be seen that when the length of the cladding tube is short, points A and B deform inside the tube, exhibiting a compressive creep deformation mode (Fig. 6, c); When the length of the cladding is long, point A deforms outside the tube and point B still deforms inside the tube, exhibiting a bending deformation mode (Fig. 6, d). The deformation results of the current work under short tube conditions are consistent with [20], and the deformation mode under long tube conditions is consistent with [11, 12].

As shown in Fig. 3, the displacement of the long-axis (U_A, black line) is slightly negative compared to that of the short-axis (U_B, blue line). Therefore, for the baseline height ($H = 20$ mm), the displacements indicate that both axes are compressed, corresponding to a compression mode (Fig. 6, c). In contrast, for longer tubes, the behavior shifts to a bending mode (Fig. 6, d). In this scenario, the short-axis exhibits negative displacement while the long-axis shows positive displacement, indicating that the tube undergoes global buckling rather than local compression. This transition is governed by both the tube length and boundary effect: 1. For short tubes: The boundary constraints are dominant, restricting lateral movement and forcing the structure into a compression mode. 2. For long tubes: The boundary effect diminishes, allowing the tube to behave like a infinite structure (under plane strain conditions), which may susceptible to buckling, manifesting as the observed bending mode.

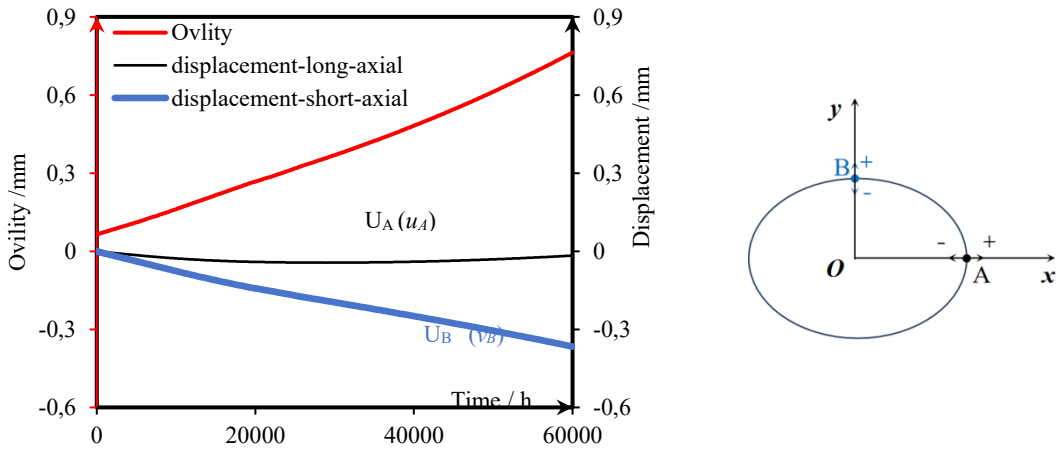

Fig. 3 Ovality and displacement curve with time (note that the negative displacements indicate the point deform to the inward of the tube)

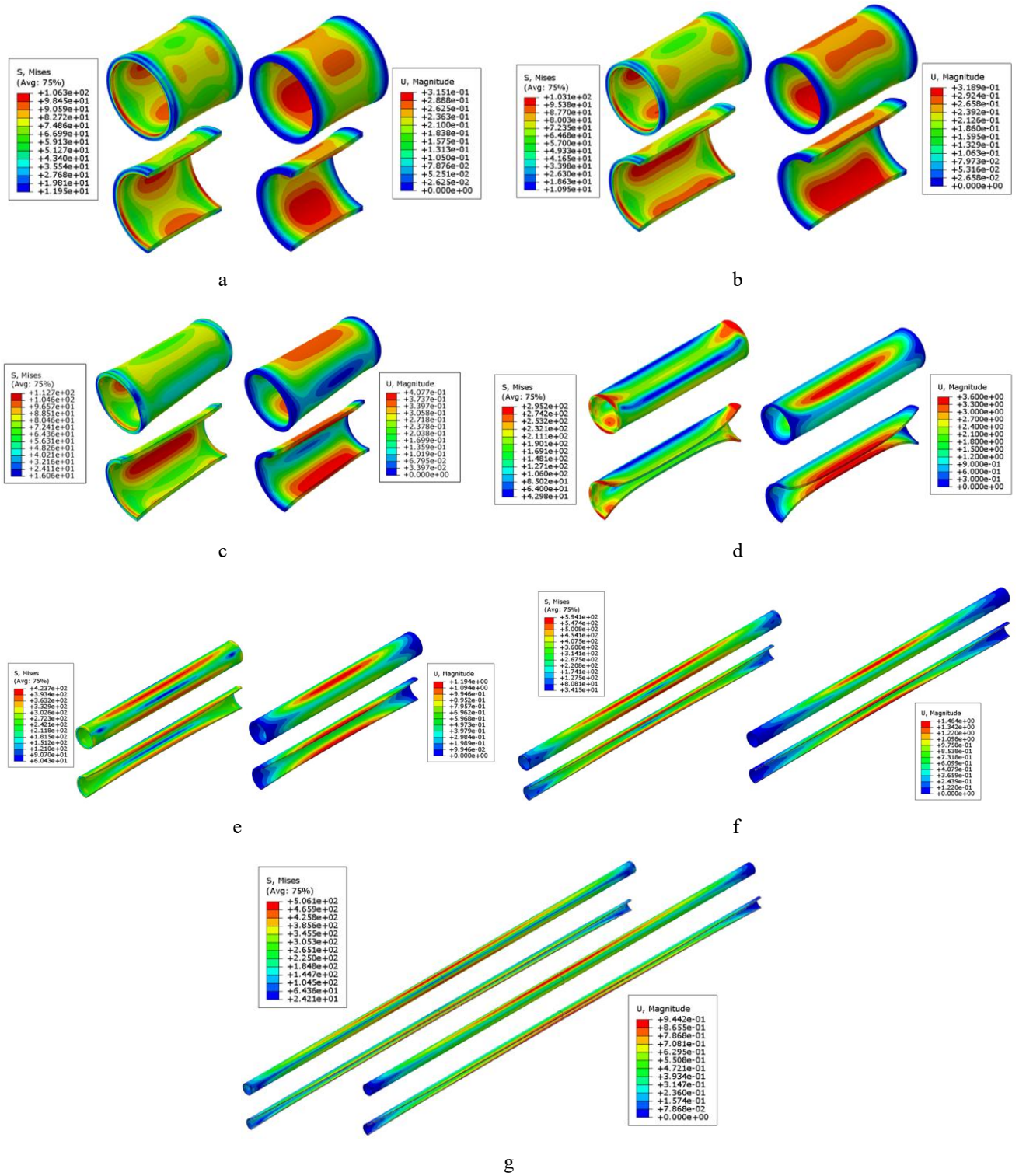

Fig. 4 Mises stress contour and displacement contour of the cladding tube for different axial length (figures on the bottom are cut views): a – height = 10 mm, t = 60000 h; b – height = 15 mm, t = 60000 h; c – height = 20 mm, t = 60000 h (baseline model); d – height = 40 mm, t = 47000 h; e – height = 80 mm, t = 7560 h (interrupted due to divergence); f – height = 200 mm, t = 5759 h (interrupted due to divergence); g – height = 400 mm, t = 5648 h (interrupted due to divergence)

3.3. Influence of cladding tube thickness

By reducing the thickness of the cladding tube to 0.45 mm and 0.33 mm for creep simulation, it was found that its deformation mode was the same as the baseline model (0.57 mm), as shown in Fig. 7. The magnitude of creep deformation is different with different thickness cases. As the thickness decreased, the stress of the tube structure gradually increased, resulting in more accumulated creep deformation. At t = 60000 h, the creep deformation became larger and larger, and the displacement of the minor axis was negative along the axial direction. The displacement of the major axis first decreased and then increased along the axial direction, and then tended to stabilize. The results of this paper are consistent with the deformation results of Zhang et al. [20].

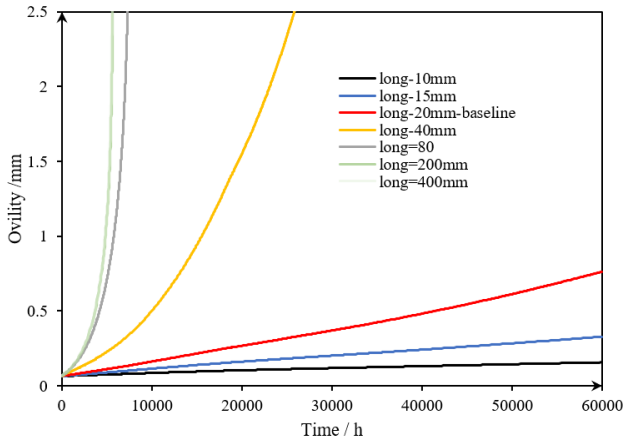

Fig. 5 The ovality-time curve of the tube with different axial lengths (for the length of 200 mm, there is no apparent difference with that of 400 mm)

3.4. The influence of boundary conditions

To restrict the rigid body motions, the boundary conditions at one end of the cladding tube should be fixed (restrict the u1, u2, and u3 of the end nodes), and the boundary conditions at the other end should also be fixed. When the axial length is *L*, the simulated real situation is the creep of the cladding tube at *L*, which is the baseline situation in this article (Case 0: baseline, height = 20mm). In this section, the following situations are compared: Case 1: The boundary conditions at the other end only restrict the axial displacement u3, height = 20 mm; Case 2: the boundary conditions at the other end are not constrained, height = 20 mm; Case 3: the other end constraints u3, r1, and r2, height = 20 mm, which indicate the effective height is 40 mm. Please see the Fig. 8 for displacement boundary conditions.

The curve of the ovality of the middle section with the maximum deformation over time is shown in Fig. 8. It can be seen that different boundary conditions have a significant impact on the ovality-time curve, and the equivalent length of the cladding tube is greater than 40mm when the other end boundary condition is free and only restricts axial displacement. Therefore, when simulating the creep deformation of the cladding tube, relevant creep experiments need to be conducted to accurately determine the boundary conditions. Generally, the length of the unsupported segment of the cladding tube does not exceed 12.7 mm, and after continuous service for 60000 hours, its creep ovality is relatively small (lower than the red curve in Fig. 9), so creep collapse generally does not occur. During the operation of the reactor, it is necessary to carry out creep deformation monitoring of the unsupported section of the cladding tube to validate the model.

Zhang [12] simulated the unconstrained state of the tube in the axial direction by relaxing the axial boundary conditions at the other end, and the results showed that relaxing the constraints would accelerate the creep deformation of the cladding. We may define the "strength" of the boundary condition to measure the restriction effect. And the strength of the boundary conditions in [12] is between

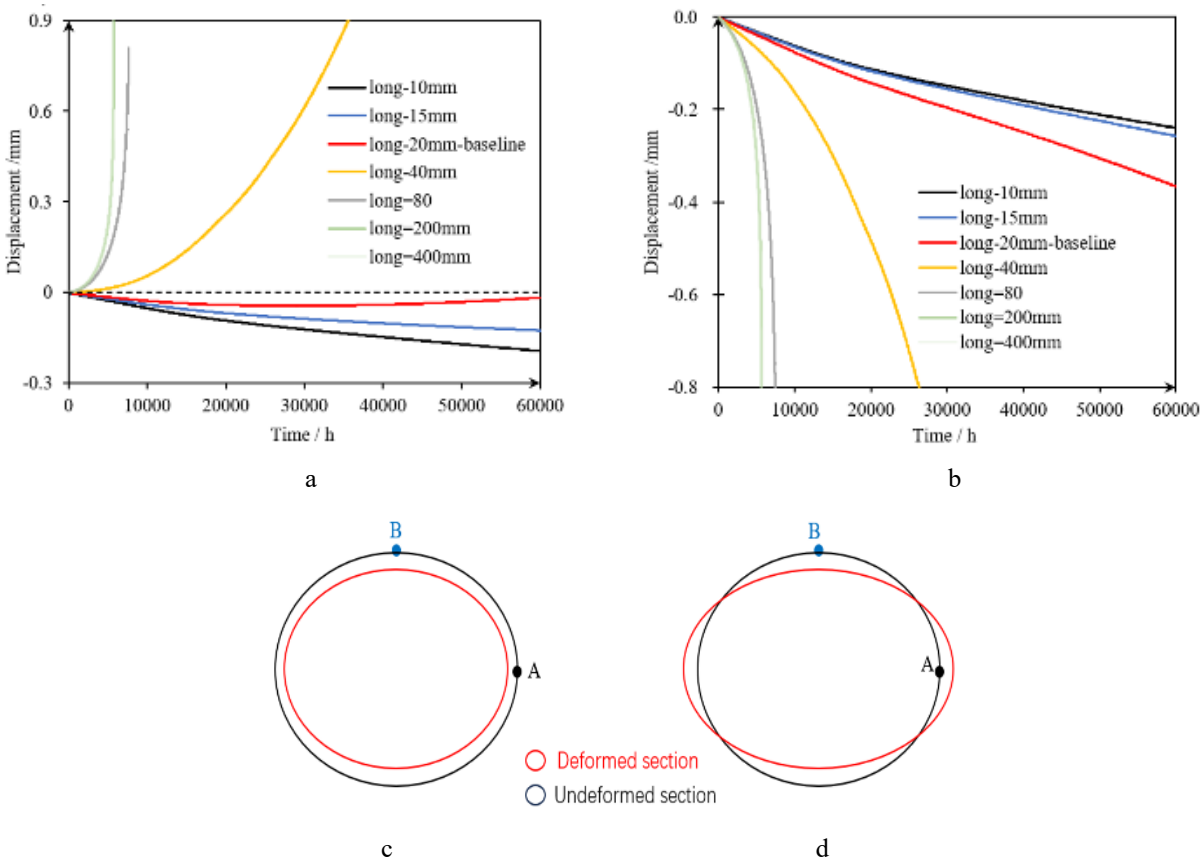

Fig. 6 Displacement-time curve of the tube with different axial length and creep deformation mode of the ovality tube: a – displacement of point A on the outer surface of the major axis, b – displacement of point B on the outer surface of the minor axis, c – deformation mode of short tube (compression mode), d – deformation mode of long tube (bending mode)

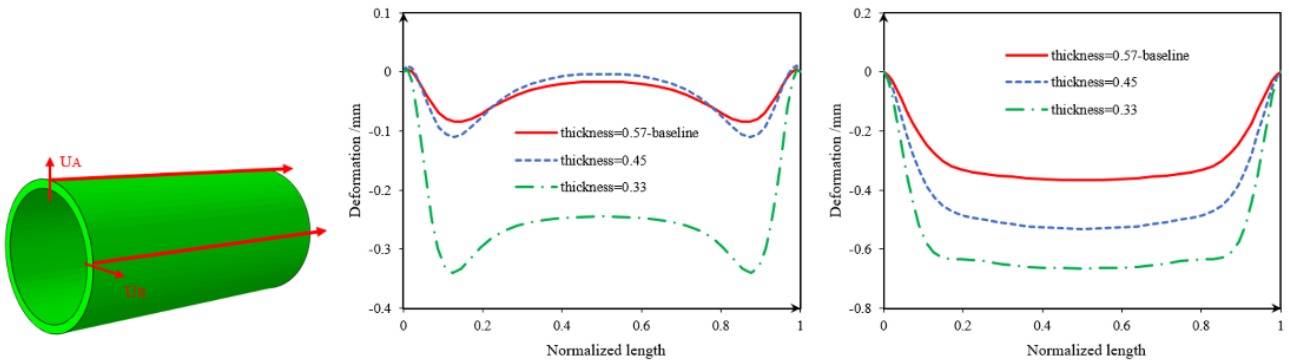

Fig. 7 Displacement along the normalized axial direction of the points on the: a – major axis and b – minor axis

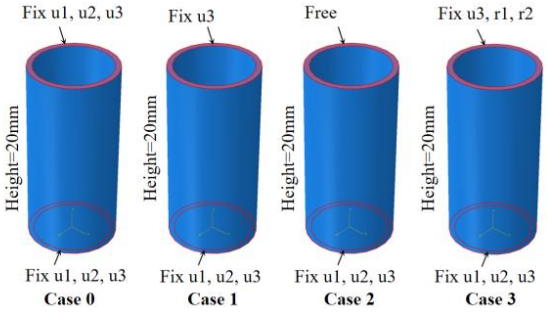

Fig. 8 Setup of the displacement boundary conditions (1, 2 and 3 correspond to x, y, z, respectively)

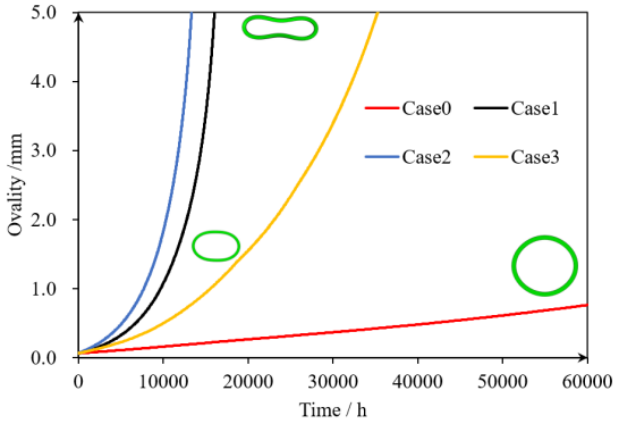

Fig. 9 Ovality-time curve of the tube with different boundary conditions (Case0: tube length 20 mm, fix u123 on two ends; Case1: tube length 20 mm, fix u123 on one end and fix u3 on the other end; Caes2: tube length 20mm, fix u123 on one end and free on the other end; Case3: tube length 20 mm, fix u123 on one end and fix u3 r1 r2 on the other end

case 0 and case 2. Different types of boundary conditions of the cladding tube do have a great influence on the creep mode and magnitude.

4. Conclusions

In this paper, we modeled the metal cladding as a finite-length tube to predict the creep deformation characteristics with the finite element method. The main conclusions are:

1. For tubes with shorter axial lengths, the points of the major axis and minor axis deform towards the interior of the tube; For longer tubes, the point on the major axis deforms outwards the interior of the tube and the point on the minor axis still deforms towards the interior of the tube.

2. When the axial length of the cladding is greater than 21 times its diameter, the cladding can be seen as an infinitely long tube from the perspective of creep deformation; For the tube with the same deformation characteristics, the correction method may be valid.

3. The boundary conditions at both ends of the cladding tube have a significant impact on its creep deformation, and the boundary conditions should be determined based on the creep experiment of the true cladding.

This study can help to design the creep deformation of the tube structure under external loading. However, there are two limitations of the current study: 1. The geometry parameters are based on the current well-used cladding tube, and the generalization of the conclusion may be validated by many sets of numerical studies (such as different radials, thickness, initial ovality, axial length) in the further work. 2. Creep experiments of the tube structure should be carried out to calibrate the boundary conditions of the computational tube model and validate the current results.

Acknowledgments

This research is supported by the Doctoral Scientific Research Foundation of Hubei University of Automotive Technology (No.202475), the Open Foundation of Key Laboratory of Automotive Power Train and Electronics (No. ZDK12024B06 and No. ZDK12025B03) and the Guiding Scientific Research Project of Shiyan (No.25Y043).

The author Z.M. would like to thank the former colleagues Li Jinggang, Huang Tao, Lu Yong and Jin Xin in China Nuclear Power Research Institute Co., Ltd for their help in modeling the cladding tube.

Author Contributions

Z.M.: Conceptualization, Methodology, Formal analysis, Investigation, Validation, Writing - original draft. L.S.: Conceptualization, Methodology, Formal analysis. F.Z.: Supervision, Conceptualization, Methodology, Writing – review & editing. H.M.: Supervision, Conceptualization, Methodology, Writing - review & editing. Z.B.: Supervision, Conceptualization, Methodology, Writing - review & editing.

Declaration of Interests

The authors declare that they have no known competing financial interests or personal relationships that could have appeared to influence the work reported in this paper.

References

1. **Cazado, M. E.; Denis, A. C.** 2018. Model of nuclear fuel pellets densification under irradiation and isothermal conditions: Application to UO 2 fuels, Journal of Nuclear Materials, 510: 585-595. https://doi.org/10.1016/j.jnucmat.2018.08.029.
2. **Yoo, J.; Oka, Y.; Ishiwatari, Y.; Liu J.** 2006. Thermo-mechanical analysis of supercritical pressure light water-cooled fast reactor fuel rod by FEMAXI-6 code, Annals of Nuclear Energy 33(17): 1379-90. https://doi.org/10.1016/j.anucene.2006.10.004.
3. **Franklin, D. G.; Adamson, R. B.** 1988. Implications of Zircaloy creep and growth to light water reactor performance, Journal of Nuclear Materials 159: 12-21. https://doi.org/10.1016/0022-3115(88)90082-7.
4. National Energy Administration. 2012. NB/T20057.3 Design of Reactor System for Pressurized Water Reactor Nuclear Power Plants. Beijing: Atomic Energy Press. 113p. Available at: https://ndls.org.cn/standard/detail/d1b4dd6e0ca687b22627e4843c71f25e.
5. **Pankaskie, P. J.** 1975. BUCKLE: an analytical computer code for calculating creep buckling of an initially oval tube. BATTELLE, PACIFIC NORTHWEST LABORATORIES. Available at: https://digital.library.unt.edu/ark:/67531/metadc1024833/.
6. **Merckx, K. R.** 1974. Calculational procedure for determining creep collapse of LWR fuel rods, Nuclear Engineering and Design 31(1): 95-101. https://doi.org/10.1016/0029-5493(74)90138-1.
7. **Mohr C. L.** 1975. COVE-1: a finite difference creep collapse code for oval fuel pin cladding material, Richland, USA: Battelle Pacific Northwest Labs. Available at: http://www.osti.gov/servlets/purl/4186018-KrivVY/
8. **Franklin, D. G.; Lucas, G. E.; Bement, A. L.** 1983. Creep of zirconium alloys in nuclear reactors, West Conshohocken, USA: ASTM International. 306p. https://doi.org/10.1520/STP815-EB.
9. **Jin, X.; Liu, X.; Lu, Y.; Deng, Y.** 2017. Introduction of fuel rod cladding creep collapse code FROCO, China Conference on Theoretical and Applied Mechanics, Beijing: Chinese Society of Mechanics: 477-482.
10. **Zhang, X.; Liu, L.; Hao, M.; Fan, Y.; Wang, P.; Huang, N.** 2016. Simulation the irradiation growth and creep of the fuel rods, Nuclear Electronics and Detection Technology 36(12): 1268-1272.
11. **Zhang, M.; Li, J.; Liu, X.; Lu, Y.; Zhu. Y.** 2022. A Bi-Layered Three-Dimensional Mechanical Modeling of the Cladding and Its Creep Deformation Analysis, Proceedings of the 2022 29th International Conference on Nuclear Engineering. Volume 2: Nuclear Fuel and Material, Reactor Physics and Transport Theory, and Fuel Cycle Technology. Virtual, Online: V002T02A004. https://doi.org/10.1115/ICONE29-88944.
12. **Zhang, M.; Luo, Y.; Lu, Y.; Zhu, Y.; Liu, X.; Li, J.; Miao, X.** 2024. On the Creep Collapse of the Cladding Considering the Irradiation Growth Effect, Proceedings of the 2023 Water Reactor Fuel Performance Meeting (WRFPM 2023), Springer Proceedings in Physics 299: 16-19. https://doi.org/10.1007/978-981-99-7157-2_2.
13. **Tang, C.; Jiao, Y.; Chen, P.; Li, Y.; Zhou, Y.** 2017. Numerical Simulation of Irradiation-Thermal-Mechanical Coupling Behaviors in Nuclear Fuel Rods, Nuclear Power Engineering 38(6): 180-184. Available at: https://www.nstl.gov.cn/paper_detail.html?id=eab7204956dac2cdccd57917f2da1468.
14. **Zhang, M.; Chen, Z.; Zhu, Y.; Lu, Y.; Liu, X.; Jin, X.; Li, J.; Luo, Y.** 2023. A Continuum-Based Degenerated Shell Element and Its Application on the Creep Deformation Analysis of Cladding, Proceedings of the Advances in Transdisciplinary Engineering 40: 60-69. https://doi.org/10.3233/ATDE230441.
15. CROV 9.4: Fuel rod collapse analysis code user's manual, FFDC05191, Rev. A, 2009.
16. **Geelhood, K. J.; Luscher, W. G.** 2014. FRAPCON-3.5: A Computer Code for the Calculation of Steady-State, Thermal-Mechanical Behavior of Oxide Fuel Rods for High Burnup (NUREG/CR-7022, Vol. 1, Rev. 1), Office of Nuclear Regulatory Research & Technical Information, Technical Reports. Available at: https://www.nrc.gov/reading-rm/doc-collections/nuregs/contract/cr7022/v1/r1/index.
17. **Hoff, N. J.; Jahsman, W. E.; Nachbar W.** 1959. A study of creep collapse of a long circular cylindrical shell under uniform external pressure, Journal of the Aerospace Sciences 26(10): 663-669. https://doi.org/10.2514/8.8243.
18. **Bargmann, H.** 1972. The lifetime of a long cylindrical shell under external pressure at elevated temperature, Nuclear Engineering and Design 22(1): 63-74. https://doi.org/10.1016/0029-5493(72)90062-3.
19. **Nishiguchi, I.; Kaji, Y.; Ioka, I.; Yamamura, T.; Yamada, Y.** 1990. A Simplified Method for Predicting Creep Collapse of a Tube Under External Pressure, ASME Journal of Pressure Vessel Technology 112(3): 233-239. https://doi.org/10.1115/1.2928619.
20. **Zhang, M.; Li, J.; Liu, X.; Lu, Y.; Zhu, Y.** 2022. Three-dimensional Mechanical Modeling of the Cladding and its Deformation Analysis Software Development, Science Technology and Engineering 22(29): 12861-12866.
21. Abaqus. 2014. Abaqus 6.14 Documentation. Available at: http://orpheus.nchc.org.tw:2080/v6.14/index.html
22. ANSYS. 2015. Ansys 16.0 Release Documentation, Theory and Modelling Guide. ANSYS Inc., Canonsburg, PA.

M. Zhang., S. Li, Z. Feng, M. Han, B. Zhang

STUDY ON THE CREEP DEFORMATION CHARACTERISTICS OF THE CYLINDRICAL TUBES UNDER EXTERNAL PRESSURE

S u m m a r y

Cylindrical tubes are fundamental structural components across many engineering fields, particularly for bearing external loads. In pressurized water reactors (PWR), the metal cladding tube acts as the first safety barrier, containing radioactive materials under extreme conditions of external pressure, high temperature, and intense fast neutron flux. Accurate prediction of its creep deformation remains a critical challenge in nuclear engineering. This study analyzes the coupled thermal and irradiation creep behavior of cladding tubes using the commercial finite element code ABAQUS and its user subroutine CREEP. The results demonstrate that creep deformation mode and magnitude are highly sensitive to geometric and mechanical factors. Specifically, longer axial lengths correlate positively with greater creep deformation, while increased wall thickness reduces it. Cladding tubes with length-to-diameter ratios exceeding 21 can be treated as infinitely long structures. Furthermore, relaxed boundary conditions have an effect equivalent to increasing the tube's effective length, thereby amplifying creep deformation. These insights are important for evaluating cladding performance and structural safety under long-term creep deformation.

Keywords: nuclear cladding, metal tube structure, creep deformation, creep collapse, finite element method.

Received October 21, 2025
Accepted April 24, 2026